Microstructures

Open Access

Supplementary Material: Topological transformation of magnetic hopfion in confined geometries

SIMULATED LTEM MAGNETIC CONTRAST OF HOPFION

Simulated LTEM images generated from micromagnetic simulation data using PyLorentz are shown in Supplementary Figure 1. Supplementary Figure 1A displays the magnetic phase shift image alongside LTEM images of a hopfion at different focus settings, including underfocus (Supplementary Figure 1B), in-focus (Supplementary Figure 1C), and overfocus (Supplementary Figure 1D). The LTEM contrast of hopfion exhibits a distinctive ring-shaped pattern that reverses under overfocus and underfocus imaging conditions.

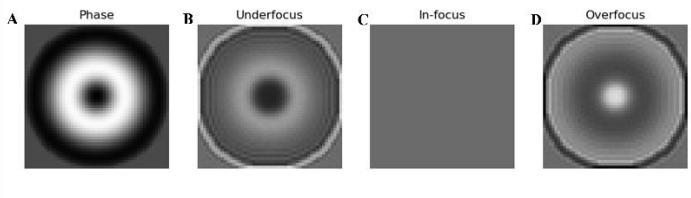

Supplementary Figure 1. Simulated LTEM images of hopfion in a nanodisk. (A) Phase-shift image, (B) under-, (C) in-, and (D) over-focus LTEM images of hopfion. The images are simulated with a defocus value of 400 μm, and the viewing directions are along the *z*-axis.

COMPARISON OF SKYRMIONIUM TUBE AND HOPFION

Recent experimental work has demonstrated that the 3D spin texture of hopfion can be distinguished from that of skyrmionium by comparing the magnetic images obtained from X-PEEM and MTXM tools. In MTXM images, both skyrmionium and hopfion exhibit a ring pattern. However, the PEEM image of hopfion shows a distinctive "ying-yang" pattern [1]. As such, hopfion hosting materials can be identified via X-PEEM images that exhibit the unique characteristics of hopfions and demonstrate their 3D spin textures from limited depths. Nonetheless, strict requirements for the sample surface and operation difficulties pose significant challenges for the observation of hopfions in bulk chiral magnets.

Off-axis electron holography (EH) is a high-resolution technique used in TEM to measure the phase shift φ of the incident electron beam and identify different magnetic structures [2, 3]. Supplementary Figure 3 presents simulated Bloch-type skyrmionium tube and hopfion structures and their corresponding phase shift images in a chiral magnet. In Supplementary Figure 2A, the skyrmionium tube is stabilized in a nanodisk with a uniform PMA value, while a hopfion (Supplementary Figure 2B) is stabilized by sandwiching the materials between two layers with strong PMA. The phase-shift images of the skyrmionium tube (Supplementary Figure 2C) and hopfion (Supplementary Figure 2D) exhibit similar ring patterns, but the maximum φ value is different for the two configurations, indicating variations in the intensity of phase shift. The phase shift of skyrmionium runs through the entire thickness of the sample, while the hopfion exhibits a finite penetration depth, resulting in a weaker phase shift. The calculated phase-shift difference $\Delta\varphi$ is significant, enabling the distinction between these two spin textures, and the potential for quantitative measurement using off-axis EH raises expectations.

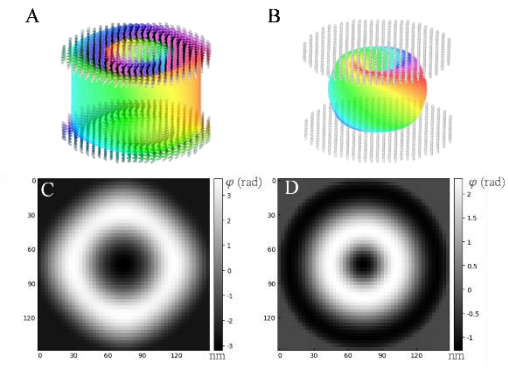

Supplementary Figure 2. Comparison of skyrmionium tube and hopfion. Preimages with $s_z = 0$ for (A) skyrmionium tube and (B) hopfion in nanodisk with a thickness of 150 nm. (C-D) Calculated phase-shift images for viewing directions along z, corresponding to the preimages in (A) and (B). The phase-shift images exhibit a similar ring pattern, but the maximum of the phase-shift value is different for the two configurations. The skyrmionium tube has a stronger phase shift than the hopfion due to its larger penetration depth.

DEMAGNETIZING ENERGY DENSITY IN ELLIPTICAL NANODISKS

The topological transformation in elliptical nanodisks is impacted by the geometric shape, which is intimately related to the demagnetization energy [4]. Demagnetizing energy density can be expressed as $\varepsilon_d = -\frac{1}{2} M_s \mathbf{B}_{\text{demag}} \cdot \mathbf{m}$. Supplementary Figures 3A–D show the distribution of demagnetizing energy density in elliptical nanodisks with different short axis length, which changes significantly as the axial ratio increases. The demagnetizing energy of hopfion is higher at the center where the spins are aligned along +z direction. This result highlights the crucial role of demagnetizing fields decided by the boundary geometry in determining the stability of hopfion, underscoring the need for careful consideration in the design of the spintronic devices based on 3D magnetic structures.

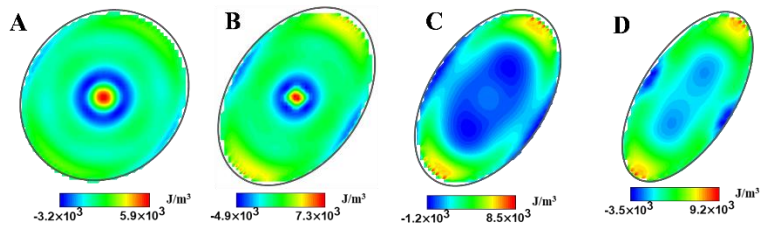

Supplementary Figure 3. (A-D) The distribution of demagnetizing energy density in elliptical nanodisks with different short axis lengths at the mid-plane.

EQUILIBRIUM DISTANCES OF HOPFION FROM THE BOUNDARY

The repulsive force from boundary can slowly push the hopfion away from the boundary. It has been demonstrated that the skyrmion-skyrmion and skyrmion-edge repulsions can change the distance between skyrmions near the boundary of racetrack [5]. The distance of hopfion from boundary can be altered in nanostripes of varying lengths. The hopfion states are obtained by relaxing an initial hopfion state located at the left side of the nanostripe under 0.34 T. The relaxed state of the hopfion in varied nanostripe lengths (l) is shown in Supplementary Figure 4A. Supplementary Figure 4B summarizes the distance (d) between the hopfion and the left edge as a function of l. The distance increases as the length becomes larger. It can be seen that d significantly increases from ~300 nm to 530 nm as l extends from 600 nm to 2100 nm. The equilibrium distance of hopfion from the boundary depends on the interplay of the magnetic interactions, especially the demagnetization related to the nanostripes shapes.

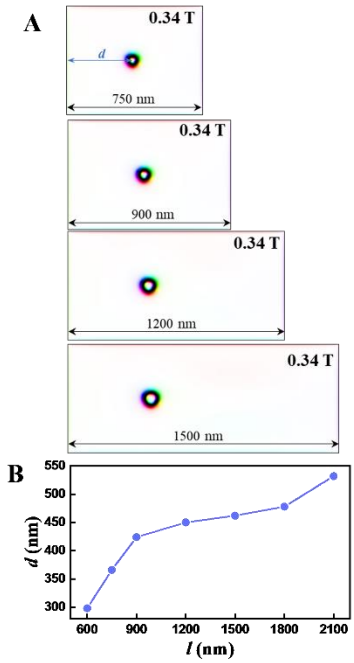

Supplementary Figure 4. (A) Relaxed hopfion state in nanostripes with different lengths. The midplane cross-sections of **m** are shown. (B) The distance (d) between the hopfion and the left edge as a function of nanostripe length (l). The nanostripe length is varied from 600 nm to 2100 nm while keeping the width constant at 600 nm.

CURRENT-DRIVEN MOTION OF TORON

As the applied magnetic field is increased from 0.34 T to 0.38 T, the hopfion undergoes a transition to a toron structure in a nanostripe. The current-driven motion of the toron structure in the nanostripe under a current density of $\mathbf{J} = -10\times 10^{11}$ A·m^{-2} is depicted in Supplementary Figures 5 A-D. The corresponding L-TEM images of the magnetic contrast during the motion of the toron are shown in Supplementary Figures 5 E-H, with a bright point at the center of the toron. The velocity components along the x and y axes (v_x and v_y, respectively) are shown in Supplementary Figure 5i, with an increase in v_y near the edge of the toron where its size is smaller. The trajectory of the toron is illustrated in Supplementary Figure 5j. The dynamic behavior of the toron structure is similar to that of the skyrmion tube, with the skyrmion Hall effect clearly observed in the toron structure.

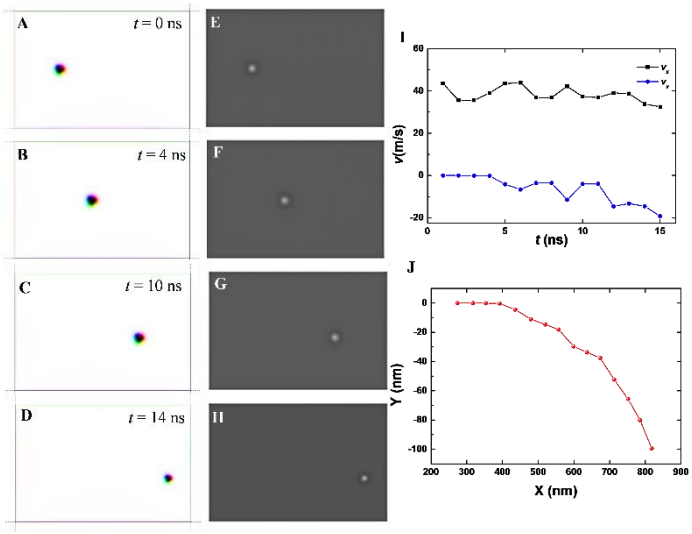

Supplementary Figure 5. Current-driven motion of a toron in a nanostripe. (A-D) Current-driven motions of a toron at J = −10× 10^{11} A·m^{-2} under a magnetic field of 0.38 T. The size of the simulated region is 900 × 600 × 100 nm^3. The midplane (z = 50 nm) cross-sections of m are shown. (E-H) Simulated under-focused LTEM images that correspond to structures in (A-D). (I) The toron motion velocity along with the x and y axes (v_x and v_y, respectively). The v_x and v_y are calculated based on spin textures in the midplane (z = 50 nm). (J) Trajectory of spin texture driven by STT during a period of 15 ns.

MOVIE 1: Hopfion motion under current at 0.34 T. The numerical simulation is conducted with (α, β) = (0.05,0.05) and a current density of **J** = −8× 10^{11} A·m^{-2}. The hopfion undergoes slight bouncing before eventually coming to a stop.

MOVIE 2: Hopfion motion under current at 0.34 T. The numerical simulation is conducted with (α, β) = (0.05,0.05) and a current density of **J** = −10× 10^{11} A·m^{-2}. The hopfion transforms into a toron state near the sample edge.

MOVIE 3: Toron motion under current at 0.38 T. The numerical simulation is conducted with (α, β) = (0.05,0.05) and a current density **J** = −10× 10^{11} A·m^{-2}. The toron motion process clearly exhibits the skyrmion Hall effect.

REFERENCES

1. Kent N, Reynolds N, Raftrey D, Campbell I T G, Virasawmy S, Dhuey S, et al, *Nat. Commun.* 2021; 12: 1562. [10.1038/s41467-021-21846-5]
2. Niitsu K, Liu Y, Booth A C, Yu X, Mathur N, Stolt M J, et al, *Nat. Mater.* 2022; 21: 305-310. [10.1038/s41563-021-01186-x]
3. Ran K, Liu Y, Guang Y, Burn D M, van der Laan G, Hesjedal T, et al, *Phys. Rev. Lett.* 2021; 126: 017204. [10.1103/PhysRevLett.126.017204]
4. Khodzhaev Z, Turgut E, *J. Phys.: Condens. Matter.* 2022; 34: 225805.
5. Zhang X, Zhao G P, Fangohr H, Liu J P, Xia W X, Xia J, et al, *Sci. Rep.* 2015; 5: 7643. [10.1038/srep07643]